Pergamon

Geochimica et Cosmochimica Acta, Vol. 67, No. 24, pp. 4807–4821, 2003

0016-7037/03 $30.00 + .00

doi:10.1016/S0016-7037(03)00207-2

Rare earth element geochemistry and petrogenesis of Miles (IIE) silicate inclusions

WEIBIAO HSU[1,2,*]

[1]Purple Mountain Observatory, Chinese Academy of Sciences, 2 West Beijing Road, Nanjing 210008, China
[2]Division of Geological and Planetary Sciences, Mail Code 170-25, California Institute of Technology, Pasadena, CA 91125, USA

(*Received August* 30, 2002; *accepted in revised form March* 6, 2003)

Abstract—An ion probe study of rare earth element (REE) geochemistry of silicate inclusions in the Miles IIE iron meteorite was carried out. Individual mineral phases among inclusions have distinct REE patterns and abundances. Most silicate grains have homogeneous REE abundances but show considerable intergrain variations between inclusions. A few pyroxene grains display normal igneous REE zoning. Phosphates (whitlockite and apatite) are highly enriched in REEs (50 to 2000 × CI) with a relatively light rare earth element (LREE)-enriched REE pattern. They usually occurred near the interfaces between inclusions and Fe host. In Miles, albitic glasses exhibit two distinctive REE patterns: a highly fractionated LREE-enriched (CI normalized La/Sm ~15) pattern with a large positive Eu anomaly and a relatively heavy rare earth element (HREE)-enriched pattern (CI-normalized Lu/Gd ~4) with a positive Eu anomaly and a negative Yb anomaly. The glass is generally depleted in REEs relative to CI chondrites.

The bulk REE abundances for each inclusion, calculated from modal abundances, vary widely, from relatively depleted in REEs (0.1 to 3 × CI) with a fractionated HREE-enriched pattern to highly enriched in REEs (10 to 100 × CI) with a relatively LREE-enriched pattern. The estimated whole rock REE abundances for Miles are at ~ 10 × CI with a relatively LREE-enriched pattern. This implies that Miles silicates could represent the product of a low degree (~10%) partial melting of a chondritic source. Phenocrysts of pyroxene in pyroxene-glassy inclusions were not in equilibrium with coexisting albitic glass and they could have crystallized from a parental melt with REEs of ~ 10 × CI. Albitic glass appears to have formed by remelting of preexisting feldspar + pyroxene + tridymite assemblage. Yb anomaly played an important role in differentiation processes of Miles silicate inclusions; however, its origin remains unsolved.

The REE data from this study suggest that Miles, like Colomera and Weekeroo Station, formed when a molten Fe ball collided on a differentiated silicate regolith near the surface of an asteroid. Silicate fragments were mixed with molten Fe by the impact. Heat from molten Fe caused localized melting of feldspar + pyroxene + tridymite assemblage. The inclusions remained isolated from one another during subsequent rapid cooling.

1. INTRODUCTION

Meteorites originate from debris of asteroids and planets, formed in the very early stages of the solar system. On the basis of their chemical compositions, meteorites fall into two categories: primitive chondrites and differentiated meteorites. Chondrites are the most primitive materials in the solar system; and they generally represent the starting compositions from which solar system objects formed. On the other hand, differentiated meteorites experienced early planetary differentiation processes (metal–silicate segregation and core formation) in asteroidal bodies. They are widely believed to have been derived from primitive chondritic materials by melting and igneous fractionation. However, the genetic links between differentiated meteorites and their chondritic precursors are largely unknown. Out of 24 differentiated groups of meteorites, most were inferred to have been derived from relatively general "chondritic" precursors (Meibom and Clark, 1999). It was difficult to specify from which group of ordinary or carbonaceous chondrites they were derived. There is only one group, the IIE iron meteorites, for which the precursor material is generally thought to have been H-chondrite-like. Study of IIE irons thus provides us with a deeper understanding of early planetary differentiation in the solar system.

IIE irons commonly contain mm- to cm-sized silicate inclusions, whose compositions range from essentially primitive (Bunch et al., 1970; Olsen and Jarosewich, 1971; Casanova et al., 1995) to strongly fractionated (Bunch et al., 1970; Wasserburg et al., 1968). The lines of evidence for a direct link between IIE silicates and H-chondrites include H-chondrite chondrules found in Netschaëvo silicate inclusions (Bunch et al., 1970; Olsen and Jarosewich, 1971) and an unmelted H-chondrite inclusion observed in Techado (Casanova et al., 1995). In addition, analyses of major element composition of Watson silicate inclusions showed that they have a whole rock composition of an H-chondrite minus the normal H-group Fe-metal and troilite content (Olsen et al., 1994). Furthermore, IIE silicates have oxygen isotopic compositions similar to those of H-group chondrites (Clayton and Mayeda, 1996). This strongly suggests that IIE irons and H chondrites were derived from a common oxygen reservoir and, perhaps, originated in the same parent body.

There exist extensive major element analyses of IIE silicate inclusions (Bence and Burnett, 1969; Bunch et al., 1970; Olsen and Jarosewich, 1971; Ikeda and Prinz, 1996; Ikeda et al., 1997; Takeda et al., 2003). These data provided vital information in our understanding of the formation of IIE irons. On the other hand, trace elements, particularly the rare earth elements

* Author to whom correspondence should be addressed (wbxu@pmo.ac.cn).

Table 1. Representative mineral chemistry of Miles silicate inclusions.

	4866-3 il							Miles silicate inclusions										
	Opx	Cpx	Ab	Trid	Chrm	Apat	Whit	Opx	Cpx	Ab	Or	Ol	Apat	Whit	Chrm	Glass	90%Ab + 10%Opx	90%Ab + 10%Trid.
SiO_2	56.37	54.09	67.97	97.70	0.00	0.00	0.00	55.86	53.86	67.62	65.65	39.49	0.00	0.00	0.00	71.63	66.44	70.63
TiO_2	0.29	0.59	0.03	0.17	1.07	0.07	0.06	0.16	0.25	0.13	0.05	0.00	0.00	0.00	4.68	0.00	0.13	0.13
Al_2O_3	0.03	0.69	19.37	1.71	0.89	0.03	0.04	0.24	1.08	20.67	18.16	0.07	0.00	0.00	1.36	16.84	18.63	18.77
Cr_2O_3	0.23	1.61	0.00	0.00	67.71	0.15	0.13	0.50	2.15	0.00	0.00	0.05	0.00	0.00	60.41	0.00	0.05	0.00
FeO	12.50	5.74	0.28	0.07	21.57	0.05	1.06	13.32	5.24	0.15	0.04	12.85	0.25	1.64	25.85	0.29	2.37	0.14
MnO	0.82	0.44	0.00	0.00	1.18	0.12	0.05	0.49	0.19	0.00	0.00	0.60	0.00	0.00	1.45	0.00	0.05	0.00
MgO	27.55	15.97	0.00	0.00	5.63	0.03	3.62	28.27	15.86	0.00	0.02	45.71	0.06	3.64	4.94	0.05	2.83	0.00
CaO	1.06	19.40	0.02	0.16	0.00	46.71	41.79	1.20	19.76	0.79	0.03	0.04	52.28	46.28	0.00	0.01	0.83	0.73
Na_2O	0.03	0.93	11.79	0.92	0.00	0.48	3.20	0.04	1.09	11.17	0.92	0.00	0.45	2.99	0.00	10.66	10.06	10.15
K_2O	0.00	0.00	0.38	0.09	0.00	0.04	0.07	0.00	0.00	0.26	15.09	0.00	0.00	0.02	0.00	0.44	0.23	0.24
ZnO					1.65										1.09			
V_2O_5					0.21													
P_2O_5					0.00	NA	NA						41.57	45.55				
Cl						NA							5.45					
Total	98.88	99.46	99.84	100.82	99.91			100.08	99.48	100.79	99.96	98.81	100.06	100.12	99.78	99.91	100.72	100.79

Data source: Ikeda and Prinz (1996) and Ikeda (2002, personal communication).

Abbreviations: Opx = orthopyroxene; Cpx = diopside; Ab = albite; Trid = tridymite; Chrm = chromite; Apat = apatite; Whit = whitlockite; Or = K-feldspar; Ol = olivine; Glass = albitic glass; NA = not analyzed.

(REEs), also play an important role in studying igneous rocks. They are the most diagnostic indicators of the processes, such as crystallization, fractionation, and differentiation, that led to the formation of igneous rocks. However, the study of trace element geochemistry, particularly the in situ REE analysis, is very limited in these meteorites (Evensen et al., 1979; Ebihara et al., 1997; Hsu et al., 1997; Ruzicka et al., 1999). As part of our continuing effort to constrain the formation of IIE irons in the early solar system, I carried out an ion probe investigation of REE geochemistry in silicate inclusions from the Miles IIE iron meteorite. A preliminary report of this work was presented by Hsu (2002).

2. ANALYTICAL TECHNIQUES

Polished thin sections of Miles (AMNH 4866-3, 4866-4, 4866-5) were examined with an optical transmission and reflectance microscope and a JEOL JSM-35CF scanning electron microscope. The selected inclusions were photographed and documented for further ion microprobe analyses. Trace element concentrations were determined with the modified CAMECA IMS-3f ion microprobe at Caltech, using the techniques described by Zinner and Crozaz (1986). Primary beam currents of 10 nA for phosphates and 20 nA for silicates were used to sputter positive secondary ions from the sample surfaces. The beam spot sizes are ~30 μm. The secondary ions were collected at a low mass resolution using 80 V of energy filtering, which efficiently suppresses complex molecular interferences (Zinner and Crozaz, 1986). Unfortunately, simple molecular ions, such as SiO^+, cannot be eliminated with this technique. A deconvolution calculation was carried out in the REE mass range to eliminate the simple molecular interferences. Some mineral phases, such as feldspar and albitic glass, have very low heavy REE (HREE) abundances that are close to or below the detection limit. In this case, Y concentration was used as an analog of HREEs. It should be noted that the $^{89}Y^+$ signal was not included in the deconvolution calculation. Therefore, Y concentration could be contaminated by the $^{40}Ca^{49}Ti^+$ molecular interference. Fortunately, these phases have very low Ca and Ti contents. The $^{40}Ca^{49}Ti^+$ ion signal is insignificant. For the first order of estimation, Y concentration obtained by the ion probe essentially represents the HREE abundances in these phases. The REE abundances are normalized to the CI chondrite values of Palme et al. (1981). Synthetic titanium-pyroxene glass, NBS-612, plagioclase glass, and Durango apatite standards were measured periodically to account for any variation of ionization efficiencies caused by minor changes of operating conditions. The reference element concentrations for each phase analyzed are taken from Table 1.

3. PETROLOGY, MINERAL CHEMISTRY, AND TRACE ELEMENT GEOCHEMISTRY

Miles contains abundant highly differentiated silicate inclusions (10 to 20 vol.%, Ikeda and Prinz, 1996). Ikeda and Prinz (1996) and Ikeda et al. (1997) performed a detailed petrographical and mineralogical study of 49 silicate inclusions in Miles (AMNH 4866-1, 2, 3, 4, 5, 6, 7, and 8). They found that these inclusions are in the size range of 2–10 mm and exhibit round, ellipsoidal, and irregular shapes. Among the inclusions they studied, most (42) are gabbroic and the remaining (7) are cryptocrystalline. Gabbroic inclusions are usually irregular in shape and contain euhedral phenocrysts of diopside, Na-feldspar, and orthopyroxene, whereas cryptocrystalline inclusions are generally round and consist mainly of albitic glass and sometimes large diopside phenocrysts. In this work, I studied seven silicate inclusions from Miles (AMNH 4866-3, 4, and 5). Their major element chemistry was previously analyzed by Ikeda and Prinz (1996). Table 1 lists some representative mineral compositions. Here I give a brief description that is pertinent to the trace element geochemical study.

Four inclusions (4866-3 i1, 4866-3 i2, 4866-3 i3, and 4866-4 i5) are coarse-grained polymineralic inclusions; inclusions 4866-4 i4 and 4866-4 i6 are pyroxene-bearing glassy inclusions; and inclusion 4866-5 i7 mainly consists of albitic glass. Among the inclusions, albitic glass and diopside ($En_{45-50}Fs_{8-12}Wo_{40-45}$) are the most abundant phases, followed by orthopyroxene ($En_{75-78}Fs_{19-23}Wo_{1-4}$) and Na-feldspar ($An_{1-15}Ab_{83-97}Or_{1-5}$). Accessory phases found in the inclusions include K-feldspar, whitlockite, apatite, chromite, and tridymite (SiO_2). The albitic glass has a composition similar to that of albite, but with excess amounts of silica. Diopside has essentially homogeneous major element compositions within a given grain but shows a small intergrain variation (e.g., Wo component from 40–45). It also displays a relatively large variation of minor element concen-

Table 2. Modal abundances of the silicate inclusions from the Miles IIE iron meteorite.

Inclusion #	Albitic glass	Diopside	Orthopyroxene	Feldspar	Whitlockite	Apatite	Chromite
4866-3 i1		60%	15%	2%	2%	19%	2%
4866-3 i2		23.5%	30%	44%			2.5%
4866-3 i3	11.5%	68%		20.5%			
4866-4 i4	46.5%	15%	28%		4.5%		6%
4866-4 i5		28%	45.5%	12%		0.5%	13.5%
4866-4 i6	60%		40%				
4866-5 i7	100%						

The modal abundances were obtained by point-counting on backscattered electron images or on reflected light microscope photos.

trations (e.g., Al_2O_3 from 0.2 to 1.3 wt.%, Ikeda and Prinz, 1996). Some orthopyroxene grains exhibit major as well as minor element chemical zoning. From the core toward the rim, MgO, Cr_2O_3, and Al_2O_3 contents gradually decrease but FeO and TiO_2 increase. Within 50 μm to the edge, the grains show reverse zoning, i.e., FeO content decreases sharply toward the edge (see Fig. 5 of Ikeda and Prinz, 1996). Whitlockite or apatite usually occurs near the boundary between silicate inclusions and metal host. The mineral modal abundances vary significantly from inclusion to inclusion. Table 2 lists mineral modal abundances of seven inclusions studied in this work. They were obtained by point-counting on backscattered electron images or on reflected light microscope photographs. A few hundred points were used in each case. The estimated errors are less than 1%. A comprehensive investigation of REE concentrations in mineral phases of these inclusions was carried out. The REE analyses of each inclusion are reported in Appendix 1.

3.1. 4866-3 i1

This is a coarse-grained polymineralic inclusion and corresponds to inclusion No. 3F (see their Fig. 1–14) of Ikeda and Prinz (1996). It consists mainly of diopside, orthopyroxene, and apatite with minor amounts of whitlockite, albite, and chromite. Their mineral chemistry is reported in Table 1. This inclusion is irregular in shape with a size of 1.2 × 2.4 mm (Fig. 1a). Diopside ($En_{48}Fs_{10}Wo_{42}$) is the major phase (60 vol.%). It is intergrown with orthopyroxene ($En_{78}Fs_{20}Wo_2$). Apatite occurs as a rather large (0.4 × 1 mm) prism at the interface between the silicate inclusion and metal host. A small whitlockite grain (150 × 300 μm) overgrows on the apatite prism. This whitlockite crystal also contains a thin tridymite rod (10 × 100 μm). REE measurements were carried out in diopside (1 analysis), orthopyroxene (1), apatite (2), and whitlockite (3). Diopside has a typical concave-downward HREE-enriched, CI-normalized REE pattern with a negative Eu anomaly (Fig. 1b). This mineral is moderately enriched in REEs relative to CI chondrites (La at ~1 × CI and Lu at ~3.7 × CI). Orthopyroxene has a highly fractionated HREE-enriched REE pattern with a negative Eu anomaly and is relatively depleted in REEs (La at ~0.03 × CI and Lu at ~1.4 × CI). Two analyses of apatite yielded essentially the same REE concentrations. This mineral has a relatively light rare earth element (LREE)-enriched REE pattern with a negative Eu anomaly and REE abundances at levels of 50 to 300 × CI. Whitlockite also has an LREE-enriched REE pattern with a negative Eu anomaly, and it is highly enriched in REEs (70 to 2000 × CI). The whitlockite grain displays a considerable intragrain variation of REE

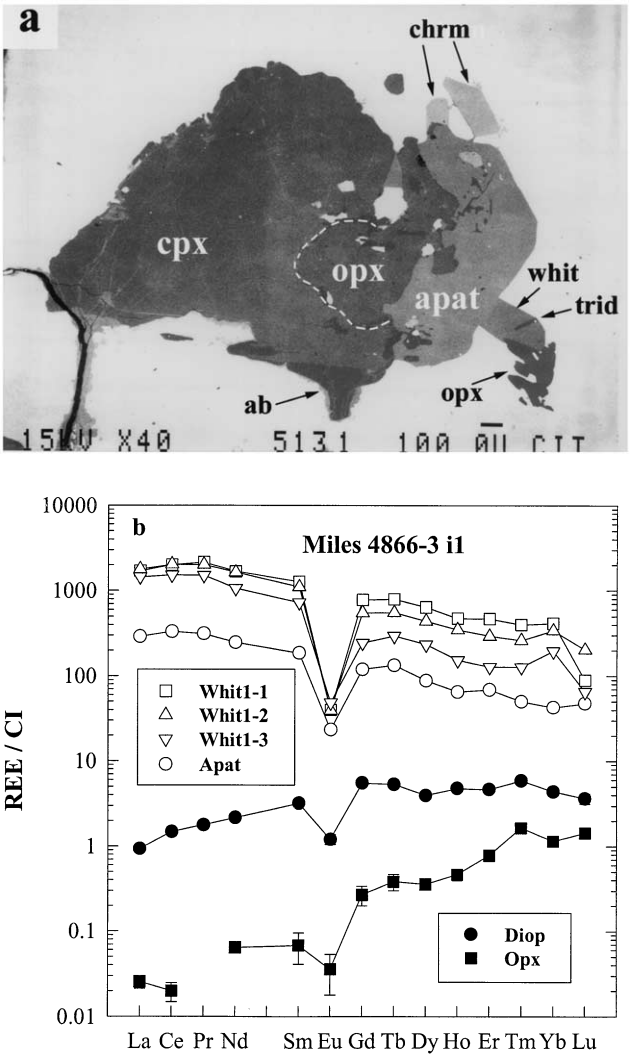

Fig. 1. (a) Backscattered electron image of the Miles 4866-3 i1 inclusion. It consists of diopside (cpx), orthopyroxene (opx), and apatite (apat) with minor amounts of whitlockite (whit), albite (ab), and chromite (chrm). The whitlockite grain contains a thin tridymite (trid) rod. (b) CI-normalized REE abundances of diopside (Diop), orthopyroxene (Opx), apatite (Apat), and whitlockite (Whit). Whitlockite displays variable REE abundances over a 200 μm distance.

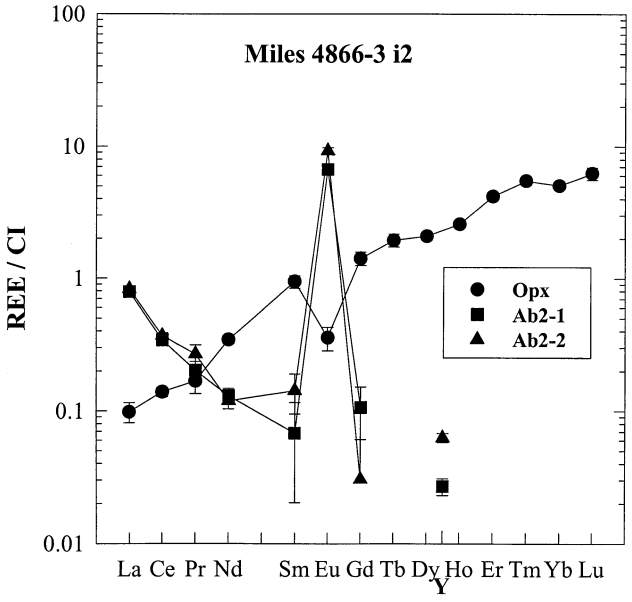

Fig. 2. CI-normalized REE abundances of orthopyroxene (Opx) and albite (Ab) from the 4866-3 i2 inclusion. The albite is homogeneous in REEs. Orthopyroxene has a highly fractionated HREE-enriched REE pattern.

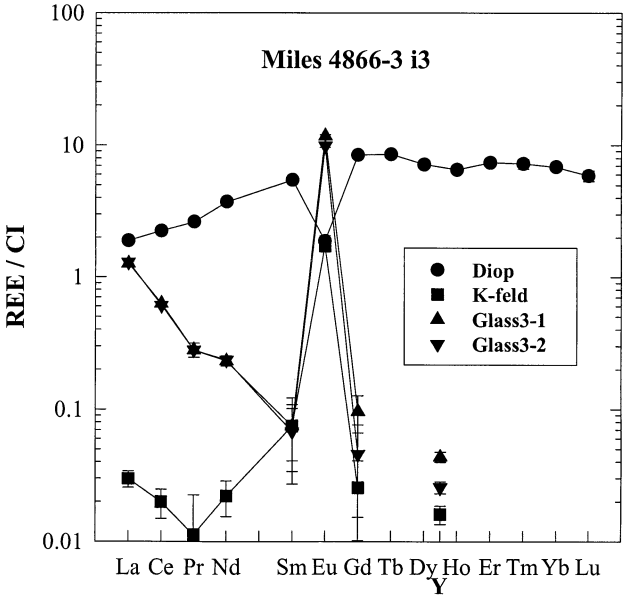

Fig. 3. CI-normalized REE abundances of diopside (Diop), K-feldspar (K-feld), and albitic glass (Glass) from the 4866-3 i3 inclusion. The glass is homogeneous in REEs. K-feldspar is extremely depleted in REEs.

concentrations despite its small size. Three analyses over a distance of 200 μm in the grain showed that LREE abundances vary by a factor of up to 2 and HREE abundances by a factor of 3. A positive Yb anomaly is noted.

3.2. 4866-3 i2

This inclusion is also coarse-grained. It is irregular in shape and has a size of 2.5 $\times$ 4 mm. The inclusion contains large crystals ($\sim$1 $\times$ 1 mm) of diopside, orthopyroxene, and feldspar. A chromite grain (400 $\times$ 400 μm) is present in the center of the inclusion. Two REE analyses were made in an albite grain and one in an orthopyroxene grain (Fig. 2). The albite grain is homogeneous in REEs and has a highly fractionated LREE-enriched REE pattern with a large positive Eu anomaly. This mineral is depleted in REEs with LREE abundances at 0.1 to 0.8 $\times$ CI and HREE abundances below the detection limit. As an analog of HREEs, Y is at 0.03 to 0.06 $\times$ CI in this mineral. Orthopyroxene has a highly fractionated HREE-enriched REE pattern with a very steep slope (CI-normalized Lu/La $\sim$65). While LREEs are relatively depleted (0.1 to 0.9 $\times$ CI) in this mineral, HREEs are generally enriched (1.4 to 6.3 $\times$ CI) relative to CI chondrites.

3.3. 4866-3 i3

This is an irregularly shaped, coarse-grained inclusion. It contains large crystals of diopside (up to 1.3 $\times$ 3.6 mm). Both Na-feldspar and K-feldspar are present in this inclusion. A round albitic glass (1 $\times$ 1.4 mm) is attached on one edge of the inclusion adjacent to a diopside grain. Ion probe REE measurements were performed in diopside, albitic glass, and K-feldspar (Fig. 3). Diopside in this inclusion has essentially the same REE abundances and pattern as the one in the inclusion 4866-3 i1. It is relatively enriched in HREEs (Lu at $\sim$6 $\times$ CI vs. La at $\sim$2 $\times$ CI). Albitic glass is homogeneous in REEs and has REE abundances and pattern similar to that of the albite grain in 4866-3 i2. It has an LREE-enriched REE pattern with a positive Eu anomaly and is generally depleted in REEs, especially the HREEs which are below the detection limit. Y is at 0.026 to 0.044 $\times$ CI. K-feldspar is extremely depleted in REEs (0.01 to 0.05 $\times$ CI) except for Eu (1.7 $\times$ CI). HREEs are below the detection limit, and Y is present at 0.016 $\times$ CI in this mineral.

3.4. 4866-4 i4

This is an ellipsoidal shaped inclusion with a size of 3 $\times$ 4 mm (Fig. 4a). Phenocrysts of orthopyroxene (up to 2 $\times$ 2.5 mm), diopside ($\sim$2 $\times$ 2 mm), and chromite (0.8 $\times$ 1.2 mm) are set in albitic glass matrix. A round whitlockite grain ($\sim$0.7 $\times$ 1 mm) is attached on the edge of the inclusion. Part of the inclusion is surrounded by schreibersite grains. Two orthopyroxene grains (Opx1 and Opx2) are present in this inclusion. To seek any REE zoning in the phenocrysts of diopside and orthopyroxene, in situ REE measurements were carried out at the core and rim of the grains. Both diopside and orthopyroxene (Opx2) display normal igneous REE zoning, i.e., REE abundances are higher at the rim than in the core region (Fig. 4b). The variation of REE abundances between the core and the rim is up to a factor of 10. In general, these two minerals have a relatively HREE-enriched REE pattern with a negative Eu anomaly. Diopside is generally enriched in REEs (0.5 to 13 $\times$ CI) whereas orthopyroxene is depleted in REEs (0.004 to 1.8 $\times$ CI) relative to CI chondrites. Diopside and Opx1 do not show any Yb anomaly, whereas Opx2 displays a large negative Yb anomaly.

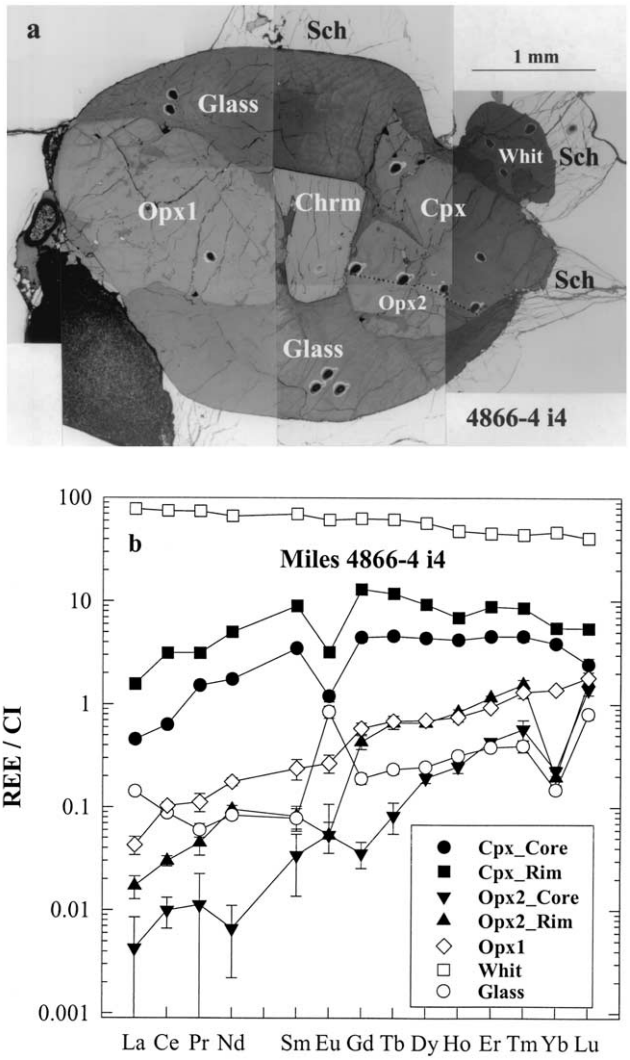

Fig. 4. (a) Reflected light photography of the Miles 4866-4 i4 silicate inclusion. Phenocrysts of diopside (Cpx), orthopyroxene (Opx1 and Opx2), and chromite (Chrm) are set in albitic glass (Glass). A whitlockite (Whit) grain is attached on the edge of the inclusion. Much of the inclusion is surrounded by schreibersite (Sch). (b) Diopside (Cpx) and orthopyroxene (Opx2) display normal igneous REE zoning, i.e., the cores have lower REEs than the rims. Whitlockite is highly enriched in REEs with a relatively LREE-enriched REE pattern. The glass is generally depleted in REEs and has a relatively HREE-enriched REE pattern with a positive Eu anomaly and a negative Yb anomaly.

Three REE measurements were performed at different locations of albitic glass. The results show that the glass is homogenous in REEs and has a relatively HREE-enriched REE pattern (CI-normalized Lu/La ~ 10) with a positive Eu anomaly and a negative Yb anomaly. The glass is generally depleted in REEs (0.06 to 0.8 × CI). Whitlockite is also homogeneous in REEs. Three REE measurements in the grain essentially yield the same REE abundances and pattern. It is enriched in REEs (40 to 80 × CI) with a relatively LREE-enriched REE pattern. The Eu anomaly is negligible. This whitlockite grain has significantly lower REEs than the one in 4866-3 i1 by a factor of more than 10.

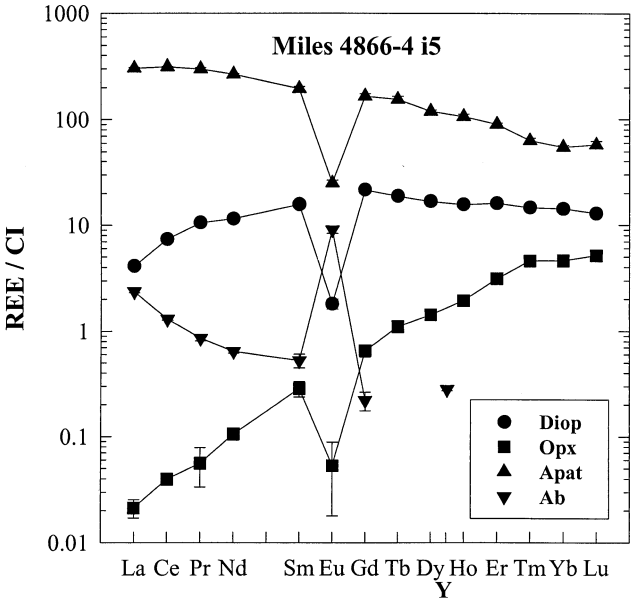

Fig. 5. REE abundances of diopside (Diop), orthopyroxene (Opx), apatite (Apat), and albite (Ab) from the 4866-4 i5 inclusion.

3.5. 4866-4 i5

This is a triangularly shaped, coarse-grained inclusion with a size of 3 × 4.5 mm. It contains crystals of diopside (28 vol.%), orthopyroxene (45.5 vol.%), albite (12 vol.%), and chromite (13.5 vol.%). A small round apatite grain (100 × 300 μm) appears on the boundary between the inclusion and metal host. Two albite grains were analyzed, and they have very similar REE abundances and pattern (Fig. 5). This mineral has an LREE-enriched REE pattern and is generally depleted in REEs (0.2 to 2.3 × CI) except for Eu (9 × CI) relative to CI chondrites. Y is present at 0.3 × CI in this mineral. Overall, albite in this inclusion has higher REE abundances than one in the 4866-3 i2 inclusion by a factor of 3. Orthopyroxene has a highly fractionated HREE-enriched REE pattern (CI-normalized Lu/La ~250) with a negative Eu anomaly. This mineral is largely depleted in LREEs (La at 0.02 × CI) and moderately enriched in HREEs (Lu at 5 × CI). Diopside has a typical concave-downward HREE-enriched REE pattern with a negative Eu anomaly. It is moderately enriched in REEs (La at ~4 × CI and Lu at ~13 × CI) and has higher REE abundances than ones in other inclusions. Apatite is highly enriched in REEs (60 to 300 × CI) and has a relatively LREE-enriched REE pattern with a negative Eu anomaly.

3.6. 4866-4 i6

This is an ellipsoidal shaped, pyroxene-bearing glassy inclusion with a size of 1 × 1.5 mm. A phenocryst of orthopyroxene (650 × 850 μm) is set in albitic glass matrix (Fig. 6a). The orthopyroxene crystal has a highly fractionated HREE-enriched REE pattern with a very steep slope (CI-normalized Lu/La ~300, Fig. 6b). This mineral is highly depleted in LREEs (La at 0.025 × CI) and moderately enriched in HREEs (Lu at ~7 × CI). Eu is below the detection limit. The albitic glass has a

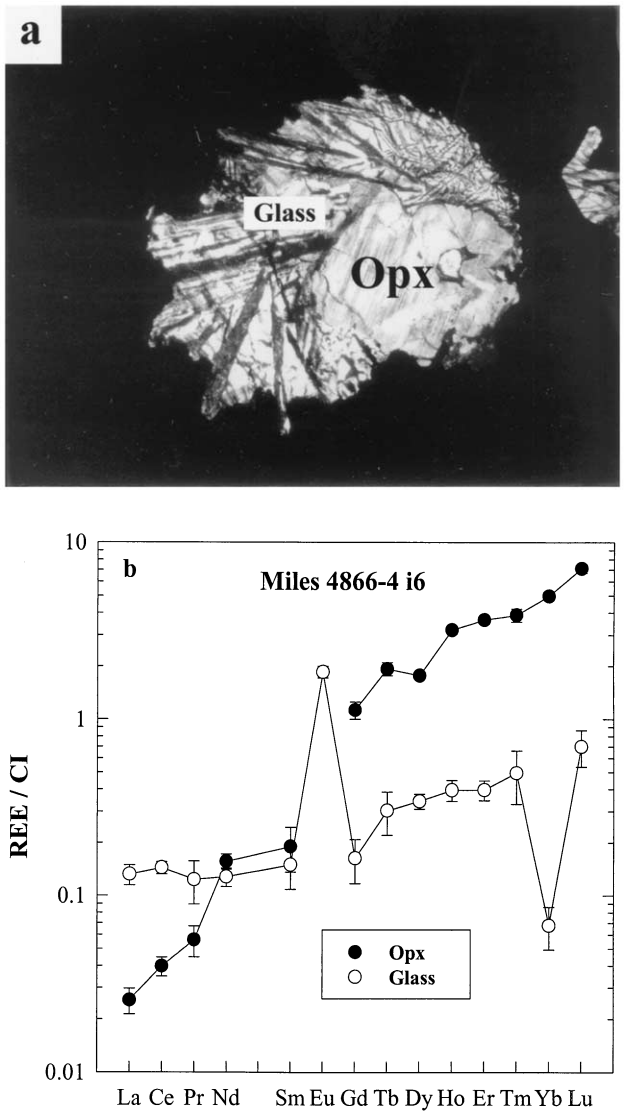

Fig. 6. (a) Transmitted light photography of the Miles 4866-4 i6 silicate inclusion. A phenocryst of orthopyroxene (Opx) is set in albitic glass (Glass). The glass is devitrified. Field of the view is 2.15 mm. (b) REE abundances of orthopyroxene (Opx) and albitic glass (Glass) from the 4866-4 i6 inclusion. These two phases do not appear in equilibrium as orthopyroxene has much higher HREE abundances than the glass and the glass displays a negative Yb anomaly.

relatively HREE-enriched REE pattern with a positive Eu anomaly and a negative Yb anomaly, which is similar to that observed in the albitic glass of the 4866-4 i4 inclusion. The glass is generally depleted in REEs (0.1 to 0.7 × CI) relative to CI chondrites except for Eu (~2 × CI).

3.7. 4866-5 i7

This is a round glassy inclusion with a diameter of ~2 mm. It is mainly composed of albitic glass. Two REE analyses yield essentially the same REE abundances and pattern (Fig. 7). It is relatively LREE-enriched with a large positive Eu anomaly (~7 × CI). The LREE abundances decrease from La (~3.5 ×

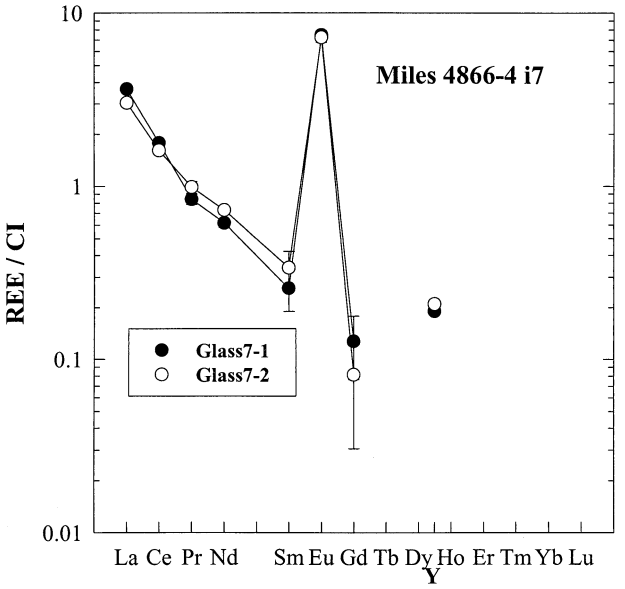

Fig. 7. REE abundances of albitic glass (Glass) from the 4866-5 i7 inclusion. The glass is homogeneous in REEs and has a REE pattern similar to that of albite.

CI) to Sm (~0.3 × CI). The HREE abundances are close to the detection limit, and their analog, Y, is at 0.2 × CI level. The REE pattern of albitic glass is similar to that of the glass in the 4866-3 i3 inclusion.

3.8. Summary of All Inclusions

Overall, individual mineral phases in different inclusions of Miles have their distinct REE patterns and abundances. Diopside has a typical concave-downward HREE-enriched REE pattern with a negative Eu anomaly. The absolute REE abundances in diopside vary from grain to grain and from inclusion to inclusion (La from 0.5 to 4 × CI and Lu from 2.5 to 13 × CI). A normal REE zoning was observed in a diopside grain of 4866-4 i4. Orthopyroxene has a highly fractionated HREE-enriched REE pattern with a very steep slope (CI-normalized La/Lu: ~40 to 300). A negative Eu anomaly is generally present, and sometimes a negative Yb anomaly is also observed. This mineral has relatively low REE abundances and shows considerable intergrain variations (La from 0.004 to 0.1 × CI and Lu from 1.4 to 7 × CI). One orthopyroxene grain of 4866-4 i4 displays normal igneous REE zoning. Feldspar has a highly fractionated LREE-enriched REE pattern with a large positive Eu anomaly. Individual Na-feldspar grains have homogenous REE abundances but show intergrain variations between inclusions (La from 0.8 to 2.5 × CI). K-feldspar has significantly lower REE abundances (0.01 to 0.03 × CI) than Na-feldspar. Two whitlockite grains were found in two inclusions (4866-3 i1 and 4866-4 i4). This mineral is highly enriched in REEs with a relatively LREE-enriched REE pattern. One grain (4866-3 i1) has higher REE abundances (La at ~1700 × CI) and displays a larger intragrain variation (Lu from 65–200 × CI) than the other (4866-4 i4, La at ~80 × CI and Lu from 38–42 × CI). Apatite is homogeneous in REEs either between

grains or within the grains. Two apatite grains from two inclusions (4866-3 i1 and 4866-4 i5) have essentially the same REE abundances (La at ~300 × CI and Lu at ~50 × CI) and pattern. It is relatively LREE-enriched with a negative Eu anomaly. In Miles, albitic glasses from four inclusions (4866-3 i3, 4866-4 i4, 4866-4 i6, and 4866-5 i7) display two distinct REE patterns. Pattern I (4866-3 i3 and 4866-5 i7) is a highly fractionated LREE-enriched (CI-normalized La/Sm ~15) REE pattern with a large positive Eu anomaly. This pattern is similar to that of Na-feldspar. Pattern II (4866-4 i4 and 4866-4 i6) is an essentially flat LREE and relatively fractionated HREE-enriched REE pattern (CI-normalized Lu/Gd ~4) with a positive Eu anomaly and a negative Yb anomaly. Glass with REE Pattern I has higher LREE abundances (La from 1.3 to 3.3 × CI and Nd from 0.23 to 0.67 × CI) than one with REE Pattern II (La from 0.02 to 0.2 × CI and Nd from 0.013 to 0.13 × CI). In general, glass is depleted in REEs relative to CI chondrites.

4. DISCUSSION

4.1. REE Budgets of Silicate Inclusions

Miles silicate inclusions have highly differentiated major element compositions. They are largely enriched in alkalies relative to H chondrites (e.g., Na_2O 4.65 wt.% vs. 0.95 wt.%, Ikeda and Prinz, 1996). It is evident that these inclusions were the products of igneous processes that included melting, crystallization, differentiation, segregation, and mixing. REEs are a powerful tool for studying igneous petrogenesis. Therefore, it is desired to know what are the bulk REE abundances in Miles individual inclusions and in the meteorite as a whole and how the REEs were partitioning in these inclusions.

In studying the REE budgets of silicate inclusions, it is critical that special attention be paid to phosphate phases. Although a minor phase, phosphate (whitlockite and apatite) is the major REE carrier in Miles silicate inclusions. It is highly enriched in REEs (up to 2000 × CI). In addition, whitlockite displays large intragrain and intergrain variations of REE abundances. Therefore, the heterogeneous distribution of whitlockite and apatite in Miles silicate inclusions would have a significant effect on their bulk REE abundances. Using the modal abundances of the inclusions listed in Table 2, I calculated the bulk REE abundances for each inclusion by combining the modal analysis with REE data for individual phases. In the case where a mineral phase was not analyzed, average REE abundances for the phase was used in the calculation. For feldspar and albitic glass, HREE abundances were estimated using Y concentration. The results of calculations are shown in Figure 8. As expected, the calculated bulk REE abundances for each inclusion vary widely, from relatively depleted in REEs (0.1 to 3 × CI) with a fractionated HREE-enriched REE pattern (e.g., 4866-4 i6) to highly enriched in REEs (10 to 100 × CI) with a relatively LREE-enriched REE pattern (e.g., 4866-3 i1). It is also noted that inclusions with phosphates (open symbols in Fig. 8) generally have higher bulk REE abundances than ones without (closed symbols). The whole rock (silicate fraction) REE abundances for Miles were estimated by averaging the data for seven inclusions studied. It is relatively LREE-enriched with REE abundances at ~ 10 × CI (see the thick line in Fig. 8). Such a REE pattern and REE abundances imply that

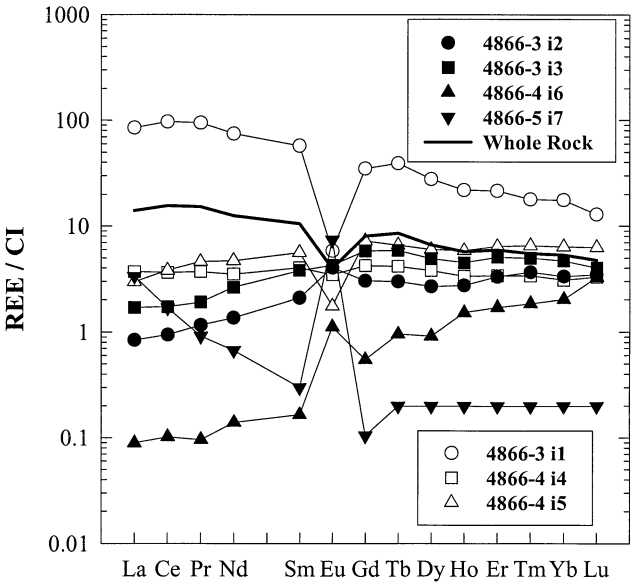

Fig. 8. Calculated bulk REE abundances for each inclusion of Miles. Inclusions with phosphates (open symbols) usually have higher bulk REE abundances than ones without (closed symbols). The whole rock REE abundances (thick line) for Miles silicates were estimated by averaging the data for each individual inclusion. It is relatively LREE-enriched with REEs at ~ 10 × CI, consistent with low degree (~10%) partial melting of a chondritic source.

Miles silicates could have been the product of a low degree (~10%) partial melting of a chondritic source.

The bulk REE abundances of silicate inclusions from IIE irons have been previously determined with instrumental neutron activation analysis (INAA) techniques (Evensen et al., 1979; Olsen et al., 1994; Ebihara et al., 1997). Evensen et al. (1979) analyzed five silicate inclusions from Weekeroo Station. These inclusions exhibit highly variable REE abundances (from 0.2 to 5 × CI) and patterns (from relatively flat to highly fractionated HREE-enriched). A silicate inclusion from Watson displays a relatively flat REE pattern with REE abundances at ~2 × CI (Olsen et al., 1994). Ebihara et al. (1997) studied nine inclusions from Miles and found these inclusions have a considerable variation of REE abundances, ranging from 0.4 to 10 × CI with an average of ~5 × CI. REE patterns for these inclusions are highly fractionated, either LREE-enriched or HREE-enriched. A positive or negative Eu anomaly is commonly present. The bulk REE abundances and patterns of silicate inclusions determined with INAA technique are very similar to what I found here and within the range estimated from the ion probe measurements. While the ion probe results and INAA measurements are compatible for most inclusions from IIE irons, a few inclusions with phosphate have significantly high bulk REE abundances estimated from ion probe analyses. These include 4866-3 i1 from Miles and CF1-A 1 i5, CF1-A 1 i6, and IIAB D1 i4 from Colomera (Hsu et al., 1997). They all have a relatively LREE-enriched REE pattern with REE abundances ranging from ~ 10 to 100 × CI. Inclusions with such high REE abundances have not been observed with INAA technique.

Questions then arise: is this mainly due to the small number of inclusions studied or is it associated with analytical tech-

niques used? There are nine inclusions from Miles analyzed with INAA and none of them has REE abundances higher than 10 × CI. Among the seven Miles inclusions studied with an ion probe, one (4866-3 i1) has high bulk REE abundances (10 to 100 × CI). Therefore, it is legitimate to ask whether the techniques used in the studies cause such a difference. As mentioned above, phosphates are the major REE carriers in IIE silicate inclusions and they usually occur as small grains near the boundaries between silicate inclusions and Fe host. It is very likely that they have been partly lost during INAA sample preparation process. Olsen et al. (1994) noted that the estimated whole rock REE abundances from the ion probe analyses are much higher than the INAA measurement of a fragment of Watson silicates. Ebihara et al. (1997) acknowledged that their INAA analyses suffered a mechanical loss of phosphates from the silicate inclusions isolated from the slab samples. Therefore, the bulk REE abundances of silicate inclusions determined with INAA are potentially lower than the real values. It should be also noted that ion probe analyses were carried out on random sections of the sample. The modal calculation from the ion probe data therefore has a potential to overestimate or underestimate the bulk REE abundances in a given inclusion due to the heterogeneous spatial (3-dimension) distribution of phosphate. In principle, the average result of a sufficiently large number of inclusions should approach the real values. The fact that the estimated whole rock (silicate fraction) REE abundances for Miles are compatible with those of the initial melt in equilibrium with the core of diopside in the 4866-4 i4 inclusion further justifies this exercise (see next section). It is therefore concluded that Miles has a whole rock (silicate fraction) REE abundances of ~ 10 × CI.

4.2. REE Balances and Equilibration Among Mineral Phases of Silicate Inclusions

The inclusion 4866-4 i4 contains several phenocrysts of diopside and orthopyroxene set in the albitic glass (Fig. 4a). Diopside (Cpx) and one orthopyroxene grain (Opx1) do not show any Yb anomaly whereas the other orthopyroxene grain (Opx2) displays a large negative Yb anomaly and the albitic glass exhibits a positive Eu anomaly and a negative Yb anomaly. It is apparent that diopside and Opx1 grains were not in equilibrium with Opx2 and the glass. They must have crystallized from a different parent melt. The general question remains as to whether equilibrium REE partitioning existed between diopside and Opx1 and between Opx2 and the glass. First, I compared the REE abundances between diopside and Opx1 and found that the abundance ratios of these two pyroxene grains are remarkably similar to the ratios of their respective REE partition coefficients determined by McKay et al. (1986) and Schwandt and McKay (1996), particularly the HREEs (Fig. 9a). The discrepancies of LREEs and Eu might be due to the large uncertainties in obtaining the concentrations in pyroxenes and their partition coefficients, because pyroxene is usually depleted in LREEs and Eu but relatively enriched in HREEs. In addition, Oe et al. (2001) recently found that REE partition coefficients for pyroxene vary with the content of minor element Al and that the variation for LREEs is much larger than that for HREEs. The Al content of pyroxenes in Miles inclusions varies by a factor of 6 (Ikeda and Prinz, 1996). Therefore,

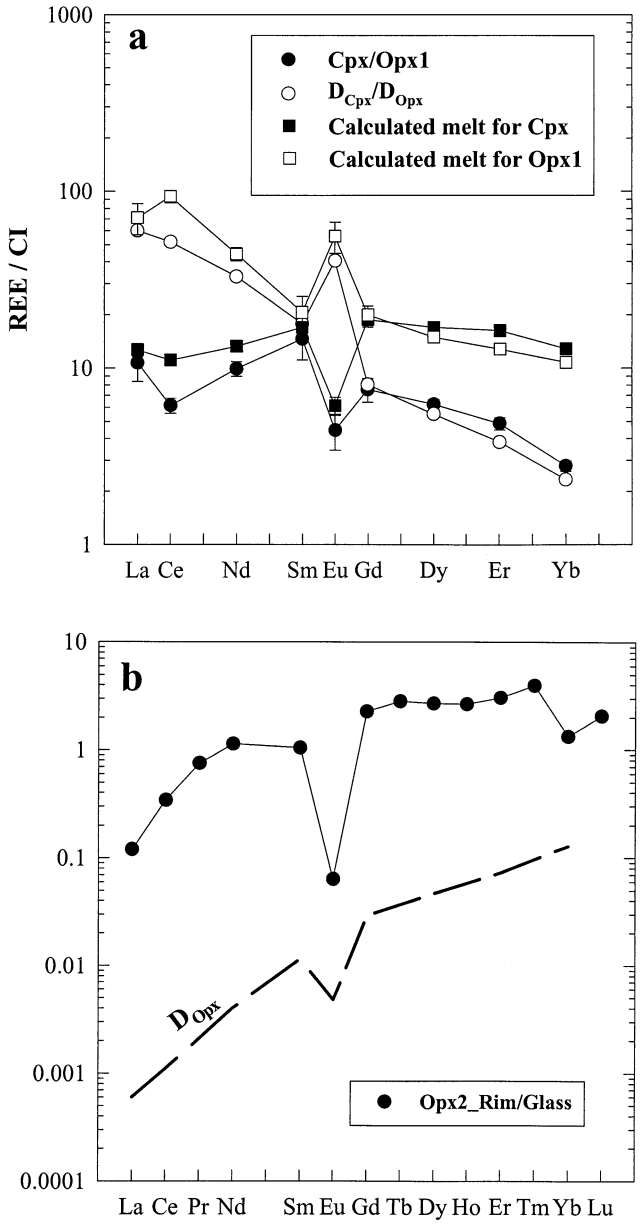

Fig. 9. (a) The REE abundance ratios (filled circles) of diopside and Opx1 are similar to the REE partition coefficient ratios (open circles) of diopside and orthopyroxene, indicating diopside and the orthopyroxene grain (Opx1) were in equilibrium and co-crystallized from a common melt. The calculated parental melt for diopside has REEs at ~ 10 × CI. (b) Comparison of REE abundance ratios of Opx2 rim and albitic glass (Opx2_Rim/Glass) with experimentally determined REE partitioning coefficients for orthopyroxene (D_{Opx}, Schwandt and McKay, 1986). The ratios are much higher than the REE partition coefficients, indicating the orthopyroxene Opx2 was not in equilibrium with the coexisting albitic glass.

it is possible that the discrepancies of LREEs and Eu could be partly due to inappropriate use of REE partition coefficients determined by McKay et al. (1986) and Schwandt and McKay (1996). Using the REE partition coefficients for diopside (D_{Cpx}) and orthopyroxene (D_{Opx}) determined by McKay et al. (1986) and Schwandt and McKay (1996), I estimated the REE abundances of the initial parental melts in equilibrium with the

cores of diopside and orthopyroxene (Opx1) (Fig. 9a). The calculated parental melt in equilibrium with the diopside core has a relatively flat REE pattern with REE abundances at ~ 10 × CI, which is remarkably similar to the whole rock REE abundances for Miles silicate inclusions. The parental melt in equilibrium with the orthopyroxene Opx1 has a relatively LREE-enriched pattern with HREEs at ~ 10 × CI. Therefore, it is highly likely that diopside and Opx1 in the 4866-4 i4 inclusion were in equilibrium and co-crystallized from the initial partial melt on Miles parent body.

I also calculated the REE abundance ratios of the orthopyroxene (Opx2) rim and the albitic glass of the 4866-4 i4 inclusion and compared the results with the REE partition coefficients for orthopyroxene (Fig. 9b). The calculated orthopyroxene/glass ratios are significantly higher by a factor of 100 than the experimentally determined partition coefficients for orthopyroxene (D_{Opx}) by Schwandt and McKay (1996). These data clearly demonstrate that the orthopyroxene Opx2 was not in equilibrium with the coexisting albitic glass in the 4866-4 i4 inclusion even though they both display a negative Yb anomaly. It must have crystallized from a different melt. The same conclusion can be obtained in the 4866-4 i6 inclusion. Therefore, it follows: 1) that diopside and orthpyroxene Opx1 grains of 4866-4 i4 co-crystallized from a parent melt with a relatively flat REE pattern and REE abundances at ~ 10 × CI; 2) that there are two different types of orthopyroxene in Miles silicate inclusions with respect to REEs, one with a negative Yb anomaly and the other without. They were not in equilibrium; 3) that coexisting albitic glass and phenocrysts of pyroxene were not in equilibrium in terms of REE partitioning; 4) that albitic glass does not represent the initial low degree partial melt from a chondritic source. A similar result was observed in Weekeroo Station silicate inclusions by Ruzicka et al. (1999).

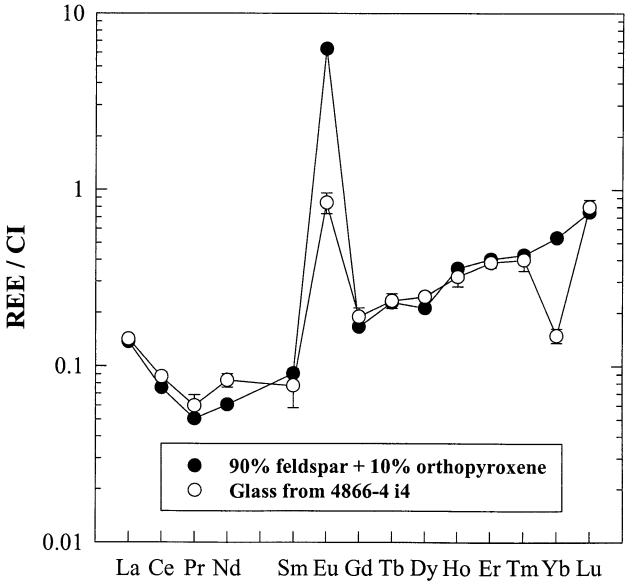

Fig. 10. Comparison of REE abundances of albitic glass from the 4866-4 i4 inclusion with a mixture of 90% feldspar and 10% orthopyroxene. The REE abundances of feldspar and orthopyroxene were taken from the median values of the observed ranges. The excellent match strongly suggests that the albitic glass in Miles silicate inclusions formed by remelting of preexisting feldspar and pyroxene.

4.3. Albitic Glass of Silicate Inclusions

Albitic glasses in silicate inclusions of Colomera, Miles, and Weekeroo Station have major element compositions similar to that of albite (Ikeda and Prinz, 1996; Ruzicka et al., 1999; Takeda et al., 2003). Chemically, it is difficult to distinguish these two phases. The albitic glass is usually round in shape within silicate inclusions. In addition, the glass shows a small range of compositional variation ($Or_{0-5}An_{0-5}$) and generally has a higher silica content (~70 wt.%) than albite. The chemical variation of glass within a given inclusion is comparable to that from one inclusion to another. A detailed scanning electron microscope study revealed that the albitic glass in Miles inclusions exhibits exsolution lamellae (Ikeda and Prinz, 1996). Micrometer-sized needles of antiperthite, anorthoclase, tridymite, and orthopyroxene are present in these glasses (see Figs. 1-8, 1-16, 1-19, and 1-20 of Ikeda and Prinz, 1996). It is evident that the electron microprobe analyses will be affected by these exsolution lamellae. This may account for the small chemical variation observed in Miles albitic glasses.

In this study, it was noted that albitic glasses display two distinct REE patterns, a highly fractionated LREE-enriched pattern (Pattern I) similar to that of feldspar and a relatively HREE-enriched pattern with a positive Eu anomaly and a negative Yb anomaly (Pattern II). In the study of silicate inclusions from Weekeroo Station, Ruzicka et al. (1999) also observed that the albitic glass has a fractionated REE pattern. They suggested that the glass might have formed by remelting of preexisting feldspar + pyroxene assemblage. Basically, they observed a good match of trace element concentrations between the glass and a mixture of 23% feldspar and 77% orthopyroxene. In this study, it was noted that feldspar in Miles has a large variation of REE abundances, LREEs ranging from 0.01 to 1 × CI. The same is true for orthopyroxene. I therefore took the median values from the ranges to represent feldspar and orthopyroxene REE abundances and found that a mixture of 90% of feldspar and 10% of orthopyroxene can produce a REE pattern remarkably similar to Pattern II (Fig. 10). The mixture also has major element compositions close to that of albitic glass (Table 1). Small discrepancies of SiO_2, FeO, and MgO contents may suggest that a few percent of silica was present in the preexisting feldspar + orthopyroxene assemblage and that Miles albitic glass contains exsolution lamellae of orthopyroxene. It is apparent that the modeling result in this study is significantly different from that of Ruzicka et al. (1999). Although the REE abundances of Weekeroo Station glass can be modeled by a 77–23 mass % mixture of average orthopyroxene and plagioclase respectively, the major element composition of the mixture differs widely from that of the glass. Ruzicka et al. (1999) suggested that FeO could be reduced during the melting event. But the large discrepancy of MgO (20 wt.% vs. <1 wt.%) remains unexplained. I believe that a 90–10 mass % mixture of feldspar and orthopyroxene is more realistic and yields an excellent match of both REE abundances and major element compositions (Fig. 10 and Table 1).

Some of the albitic glasses in Miles silicate inclusions (e.g., 4866-5 i7) display a highly fractionated LREE-enriched pattern

(Pattern I) similar to that of feldspar. One might ask whether the analyzed phase is actually feldspar. Petrographically, they are round in shape. Optically, they reveal minimally devitrified textures. These glasses can also be modeled as remelting of preexisting feldspar + orthopyroxene + tridymite assemblage. However, in this case, the amount of orthopyroxene involved in the melting event is zero. The glass therefore basically inherited the REE pattern of feldspar because tridymite is essentially free of REEs. The major element composition of a mixture of 90% feldspar + 10% tridymite is remarkably similar to that of glass (Table 1).

It now appears to be a common phenomenon that albitic glasses in IIE silicate inclusions represent the product of remelting of preexisting feldspar + pyroxene + SiO_2 assemblage. The amount of pyroxene in the assemblage varies from zero to a few percent, which results in two distinct REE patterns observed in Miles albitic glasses.

4.4. Yb Anomaly

Despite the excellent match of REE abundances between albitic glass and the mixture of feldspar and pyroxene, a discrepancy of Yb and, to a lesser extent, Eu is notable (Fig. 10). In fact, Yb anomalies were commonly observed in silicates and phosphates of IIE irons (Armstrong et al., 1990; Hsu et al., 1997; this work). Yb as well as Eu is relatively volatile compared to the other REEs (Lodders and Fegley, 1993). It is thus possible that Yb anomaly could be the product of processes that involved either condensation or evaporation (Armstrong et al., 1990). I consider this mechanism is highly unlikely for the Yb anomaly observed in IIE silicate inclusions. Laboratory evaporation experiments showed that more than 50% of material has to be evaporated in order to produce a measurable Yb anomaly (Floss et al., 1998). Such a large degree of evaporation contradicts the fact that IIE silicates are extremely rich in highly volatile alkalies. I thus consider an alternative mechanism for the observed Yb anomaly. In nature, REEs usually occur in trivalent state. Under highly reducing conditions, Eu and Yb can be divalent because of the enhanced stability of the half-filled (Eu^{2+}) and completely filled (Yb^{2+}) 4f subshell. Divalent REEs have larger ionic radii than trivalent ones and will behave differently during igneous fractionation and crystallization. This results in Yb and Eu anomalies. Yb anomaly was previously observed in unequilibrated enstatite chondrites (Hsu and Crozaz, 1998). In these meteorites, enstatite sometimes is depleted in Yb and oldhamite is enriched in Yb relative to other REEs. These meteorites are believed to have formed under highly reducing conditions. Due to the lack of experiments and thermodynamic data, it is not clear under what redox conditions Yb^{2+} will dominate in melts. The estimated oxygen fugacity for Miles silicate inclusions are $10^{-13.5}$ bars at 1500 K, $10^{-16.5}$ bars at 1300 K, and $10^{-23.5}$ bars at 1000 K (Ikeda and Prinz, 1996). In IIE irons, Fe metal, phosphates, phosphide (schreibersite), and silicates coexist. This mineral assemblage is very similar to that of pallasites (Buseck, 1977). Therefore, these two groups of meteorites should experience similar redox conditions. Yet, mineral phases (e.g., phosphates) in pallasites did not display any Yb anomaly (Davis and Olsen, 1991). Even if IIE silicate inclusions formed under highly reducing conditions, the positive Yb anomaly of whitlockite is hard to understand. Because Yb^{2+} will behave like Eu^{2+} during REE partitioning between phosphate and a melt, a negative Yb anomaly is expected. The origin of Yb anomalies in IIE silicate inclusions remains unsolved.

The Yb anomaly reflects a special process during the differentiation of IIE silicate inclusions. It is noted that diopside and most orthopyroxene grains in Miles silicate inclusions do not display any Yb anomaly. The Yb anomaly often occurs in albitic glass (negative), phosphate (positive), and a few orthopyroxene grains (negative). As discussed above, albitic glass was the result of a secondary remelting process. Yb was most likely redistributed between albitic glass and metamorphic phosphate during this process that produced excess amounts of phosphate (see below). It is evident that formation of IIE silicates involved two major igneous fractionation processes. The primary one generated a differentiated mineral assemblage of diopside, orthopyroxene, and feldspar which did not have any Yb anomaly, and the second remelting process produced albitic glass and excess amounts of metamorphic phosphate. The Yb anomaly set a mark on the later event. However, the mechanism that originated this anomaly remains to be seen.

4.5. Formation of IIE Silicate Inclusions

It is generally believed that IIE silicates were derived from an H chondrite-like precursor, but a variety of origins have been proposed (Wasserburg et al., 1968; Bunch et al., 1970; Wasson and Wang, 1986; Hsu et al., 1997; Birck and Allègre, 1998; Takeda et al., 1998; Ruzicka et al., 1999; Snyder et al., 2001; Takeda et al., 2003). In the original work on Colomera silicate inclusions, Wasserburg et al. (1968) proposed that Colomera might have originated as plums of irons in a pudding of silicates. These authors found the large exterior phenocrysts (one with an 11-cm sanidine crystal) on the surface of Colomera and suggested that Colomera was originally formed as a local molten iron segregation contained within a silicate matrix. Partial melting and differentiation near the surface of the parent body produced alkali-rich silicate inclusions in Colomera. Bunch et al. (1970) suggested that IIE irons have an origin of trapping of old silicates by “young” iron melts. In a study of siderophile elements in IIE irons, Wasson and Wang (1986) found that the metal hosts of IIE irons have limited variations of siderophile contents and show weak correlations between siderophiles and nickel. They argued that IIE irons formed as individual pools of impact-produced melt in the near-surface region of a chondritic parent body. The impact energy caused melting of metal and silicate phases and their mixing within the melt pools. The rapid cooling near the surface environment prevented the gravitational separation of these immiscible phases. Despite such differences in opinion, these authors generally agreed that IIE irons and their silicate inclusions are cogenetic and they were the products of differentiation within the same parent body.

The single parent body differentiation model for the formation of IIE irons encounters several difficulties. Mainly, it was noted that IIE silicates define two distinct groups in terms of chronological ages. Kodaïkanal, Netschaëvo, and Waston contain younger silicates (3.7 ± 0.2 Ga, Burnett and Wasserburg, 1967; Niemeyer, 1980; Olsen et al., 1994), whereas Colomera,

Miles, Techado, and Weekeroo Station have older ones (4.5 ± 0.1 Ga, Sanz et al., 1970; Casanova et al., 1995; Bogard et al., 2000). It is difficult to envision that a major magmatic activity in a small asteroidal body lasted for 0.8 Ga after the formation of the solar system. It was further noted that Kodaïkanal silicate inclusions have a Rb-Sr age of 3.8 Ga (Burnett and Wasserburg, 1967) whereas its metal host has a Re-Os age of 4.6 Ga (Birck and Allègre, 1998). It is possible that Kodaïkanal originated when old metal collided and mixed with "modern" silicates (Birck and Allègre, 1998). In a study of Hf-W isotopic composition of Watson, Snyder et al. (2001) found that its silicate inclusions and Fe host do not appear to be in equilibrium as if they would experience silicate–metal fractionation in the same parent body. This strongly suggested that the metal host and silicate inclusions in Watson were derived from two different parent bodies that collided. Differentiation within a single body model is also not compatible with the REE distributions in IIE silicates. In Miles and Weekeroo Station, phenocrysts of pyroxene and feldspar could have crystallized from initial parental melts generated by internal partial melting or an impact event. However, the chemical compositions of albitic glass require a second heating event to remelt preexisting feldspar and pyroxene. Presumably, this could be a shock event. Yet, evidence of severe shock is rare in pyroxene-glassy inclusions of Colomera, Miles, and Weekeroo Station.

As an alternative, a collision model was proposed to account for the formation of IIE irons (Hsu et al., 1997; Birck and Allègre, 1998; Takeda et al., 1998; Ruzicka et al., 1999; Snyder et al., 2001). Hsu et al. (1997) found that individual inclusions in Colomera have distinctive mineralogy, model abundances, and bulk REE concentrations. They suggested that Colomera originated when molten Fe was injected into a silicate regolith near the surface of an asteroid. Heat from molten Fe caused localized melting of silicate minerals, and blobs of melt were incorporated into the molten Fe. Once they were incorporated into the molten Fe, the inclusions remained isolated from one another during the rapid cooling period. Rapid solidification near the surface region enabled the molten Fe to entrap the silicate inclusions. Each individual inclusion would have distinctive bulk REE abundances and mineral assemblage. In this case, the metallic matrix represents the molten Fe mass and the silicate regolith was the source of silicate inclusions entrapped in Colomera. With regard to the molten Fe, it is expected that the interior of any chondritic body of radius greater than 10 km could be melted in a short time period after the formation of the solar system, if ^{26}Al was present at levels of $^{26}Al/^{27}Al \sim 1–5 \times 10^{-5}$. Collisions between such small planetesimals could release molten Fe masses that could be emplaced on or near planetary surfaces after collision. As for the silicate regolith, it could be primitive undifferentiated H-chondrite-like material as in the cases of Netschaëvo and Techado (Olsen and Jarosewich, 1971; Casanova et al., 1995) or it could be already differentiated silicates from a H-chondrite affinity as in the cases of Colomera, Miles, and Weekeroo Station (Hsu et al., 1997; Ruzicka et al., 1999; this work).

The REE abundances and patterns in Miles silicate inclusions can be well understood in the view of a collision model. The whole rock REE abundances for Miles silicate inclusions are $\sim 10 \times$ CI. This strongly suggests that the silicate regolith on the Miles parent body was highly differentiated. A low degree ($\sim$10%) partial melting of chondritic material (probably H-chondrite-like) would produce a partial melt with REEs of $\sim 10 \times$ CI. Subsequently, pyroxenes and feldspar, followed by phosphate, crystallized from the melt to form a differentiated silicate regolith. This is consistent with the fact that the calculated melt in equilibrium with diopside and orthopyroxene has REEs similar to the whole rock REE abundances of Miles silicate inclusions. Additional pieces of evidence for a differentiated silicate regolith on the Miles parent body include the observation of rare occurrence of olivine (Ikeda and Prinz, 1996) and the presence of coarse-grained minerals (diopside and orthopyroxene) in pyroxene-glassy inclusions. Partial melting of a chondritic body would produce a differentiated crust and leave olivine behind in the mantle region. The impact event occurred near the surface of an asteroid. Therefore, the mixing process would not sample olivine in the mantle region. The olivine grains seen in the Miles inclusions may represent the rare relict grains during the differentiation process. Some mineral grains (e.g., diopside and orthopyroxene) in pyroxene-glassy inclusions are euhedral and large in size (up to 2 mm). As far as the REEs are concerned, these minerals did not crystallize from coexisting albitic glass. They were in equilibrium with a parental melt with REEs similar to the whole rock REE abundances of Miles silicate inclusions. Therefore, they represented preexisting crystals originally formed during the planetary differentiation and remained intact during the secondary remelting process of feldspar and pyroxene by the injection of molten Fe.

When a molten Fe mass collided onto a differentiated silicate regolith on the Miles parent body, silicate fragments were mixed with molten Fe by the impact. The energy from the impact and the heat from the molten Fe preferentially melt the preexisting feldspar–pyroxene–SiO_2 assemblage to generate albitic glass seen in the Miles silicate inclusions. These glasses have major and trace element concentrations that are compatible with remelting of an assemblage of albite and a small but variable amount of pyroxene. The remelting process was not completed as phenocrysts of pyroxene commonly occur in pyroxene-glassy inclusions. Coarse-grained polymineralic inclusions usually do not contain albitic glass and often occur in irregular shapes. They probably represent the original silicate regolith on the Miles parent body.

Phosphate would also have been melted during this process as it has a relatively low melting point. It is noted that IIE silicates have more than a factor of 2 enrichment of phosphates, which is higher than any known H chondrites (Olsen et al., 1994; this work). In comparison with eucrites, a group of differentiated meteorites which are also believed to have formed by a low degree of partial melting of chondritic material (Hsu and Crozaz, 1996), phosphates in IIE iron silicate inclusions are much larger in size (up to several mm vs. several 10s μm in eucrites) and usually occur near the boundaries between the silicate inclusions and Fe host. Phosphates in IIE irons have relatively low REEs ($\sim$100 to 1000 $\times$ CI) compared to those of eucrites (1000 to 10000 $\times$ CI, Hsu and Crozaz, 1996). This is compatible with the formation of excess amounts of metamorphic phosphate by redox reactions between silicates and phosphorus dissolved in Fe host (Ikeda et al., 1997). Phosphorus from schreibersite and iron metal could have reacted with CaO from pyroxenes to form phosphates (Ikeda et al., 1997). Pre-

existing phosphates mixed with those formed via redox reactions that resulted in large phosphate grains seen in the 4866-3 i1 inclusion (Fig. 1a). The whitlockite grain in the 4866-3 i1 inclusion displays a relatively large intragrain variation of REEs. This may suggest that the mixing process was not completed during redox reactions under subsolidus conditions.

The second remelting process (injection of molten Fe) is most likely responsible for the Yb anomaly observed in albitic glass and phosphate of Miles silicate inclusions. Yb was redistributed between albitic glass and phosphate and preferentially incorporated into phosphate during this process. Each individual inclusion may act as a closed system as the estimated bulk REEs for Miles inclusions show no apparent Yb anomaly. The molten Fe cooled rapidly to prevent the segregation of immiscible silicate inclusions in the surface environment. The inclusions remained isolated from one another during the rapid cooling period. Each individual inclusion would have distinctive mineral assemblage and therefore bulk REE abundances.

5. CONCLUSIONS

Miles contains numerous highly differentiated silicate inclusions, which generally fall into three categories: glassy, pyroxene-glassy, and coarse-grained polymineralic. Glassy and pyroxene-glassy inclusions are in round or ellipsoidal shapes whereas polymineralic ones are usually irregular. Among the inclusions, albitic glass and diopside are the most abundant phases, followed by orthopyroxene and feldspar. Minor phases include chromite, whitlockite, and apatite. Phosphate usually occurs near the boundary between inclusions and Fe host, and its modal abundance in Miles is relatively high compared to that of ordinary chondrites.

Individual mineral phases have their distinct REE patterns and abundances. Most mineral grains have homogeneous REEs but show considerable intergrain variation. A few diopside and orthopyroxene grains display normal REE zoning. REEs vary by a factor of 10 to 100 in feldspar, 3 to 10 in diopside, 10 to 100 in orthopyroxene, and 5 to 10 in phosphate. Phenocrysts of pyroxene in pyroxene-glassy inclusions were not in equilibrium with coexisting albitic glass, but might have crystallized from a parent melt with REEs similar to the Miles whole rock REEs. The albitic glass represents a melting product of preexisting feldspar and pyroxene. Yb anomaly was observed in albitic glass, phosphate, and orthopyroxene. It may be associated with a remelting process that generated albitic glass and excess amounts of metamorphic phosphate. The origin of this anomaly remains to be seen. The estimated bulk REE abundances for seven Miles inclusions are highly variable with fractionated REE patterns. The whole rock (silicate fraction) REE abundances, calculated by averaging bulk REEs of seven inclusions, are relatively LREE-enriched with REEs of $\sim 10 \times$ CI.

The REE abundances and distributions in silicate inclusions are consistent with an origin of Miles by a collision between molten Fe and differentiated silicate regolith on its parent body. A low degree ($\sim$10%) partial melting on the Miles parent body resulted in a differentiated regolith. A molten Fe ball was injected on the surface and mixed with silicate fragments. The energy from the impact and the heat from the molten Fe preferentially melt the preexisting feldspar–pyroxene–SiO_2 assemblage to generate albitic glass seen in glassy or pyroxene-glassy inclusions. Excess amounts of phosphate were also produced by redox reactions between phosphorous from molten Fe and CaO from pyroxene. Once they were incorporated into the molten Fe, the inclusions remained isolated from one another during the rapid cooling period near the surface region. Each individual inclusion would have distinctive bulk REE abundances and mineral assemblage.

Acknowledgments—The thin sections studied were provided by the American Museum of Natural History. The author would like to thank Dr. Yukio Ikeda for helpful discussions and for permission to use his unpublished electron microprobe data of Miles silicate inclusions. He also acknowledges constructive reviews by A. Ruzicka, A. M. Davis, A. Brandon, G. Kurat, H. Palme, and an anonymous reviewer. The author thanks the support of the "One-Hundred-Talent Program" of the Chinese Academy of Sciences.

Associate editor: A. Brandon

REFERENCES

Armstrong J. T., Kennedy A. K., Carpenter P. K., and Albee A. L. (1990) Petrography and trace element chemistry of Colomera (IIE) silicate inclusions: Rhyolitic plums in the pudding. *Lunar Planet. Sci. Conf.* **XXI**, 22–23.

Bence A. E. and Burnett D. S. (1969) Chemistry and mineralogy of the silicates and metal of the Kodaikanal meteorite. *Geochim. Cosmochim. Acta* **33**, 387–407.

Birck J. L. and Allègre C. J. (1998) Rhenium-187–osmium-187 in iron meteorites and the strange origin of the Kodaïkanal meteorite. *Meteoritics Planet. Sci.* **33**, 647–653.

Bogard D. D., Garrison D. H., and McCoy T. J. (2000) Chronology and petrology of silicates from IIE iron meteorites: Evidence of a complex parent body evolution. *Geochim. Cosmochim. Acta* **64**, 2133–2154.

Bunch T. E., Keil K., and Olsen E. (1970) Mineralogy and petrology of silicate inclusions in iron meteorites. *Contr. Mineral. Petrol.* **25**, 297–340.

Burnett D. S. and Wasserburg G. J. (1967) Evidence for the formation of an iron meteorite at 3.8×10^9 years. *Earth Planet. Sci. Lett.* **2**, 137–147.

Buseck P. R. (1977) Pallasite meteorites—mineralogy, petrology, and geochemistry. *Geochim. Cosmochim. Acta* **41**, 711–740.

Casanova I., Graf T., and Marti K. (1995) Discovery of an unmelted H-chondrite inclusion in an iron meteorite. *Science* **268**, 540–542.

Clayton R. N. and Mayeda T. K. (1996) Oxygen isotope studies of achondrites. *Geochim. Cosmochim. Acta* **60**, 1999–2017.

Davis A. M. and Olsen E. J. (1991) Phosphates in pallasite meteorites as probes of mantle processes in small planetary bodies. *Nature* **353**, 637–640.

Ebihara M., Ikeda Y., and Prinz M. (1997) Petrology and chemistry of the Miles IIE irons. II. Chemical characteristics of the Miles silicate inclusions. *Antarct. Meteorite Res.* **10**, 373–388.

Evensen N. M., Hamilton P. J., Harlow G. E., Klimentidis R., O'Nions R. K., and Prinz M. (1979) Silicate inclusions in Weekeroo Station: Planetary differentiates. *Lunar Planet. Sci.* **X**, 376–378.

Floss C., El Goresy A., Zinner E., Palme H., Weckwerth G., and Rammensee W. (1998) Corundum-bearing residues produced through the evaporation of natural and synthetic hibonite. *Meteoritics Planet. Sci.* **33**, 191–206.

Hsu W. and Crozaz G. (1996) Mineral chemistry and the petrogenesis of eucrites: I. Noncumulate eucrites. *Geochim. Cosmochim. Acta* **60**, 4571–4591.

Hsu W. and Crozaz G. (1998) Mineral chemistry and the origin of enstatite in unequilibrated enstatite chondrites. *Geochim. Cosmochim. Acta* **62**, 1993–2004.

Hsu W., Takeda H., Huss G. R., and Wasserburg G. J. (1997) Mineralogy and chemical compositions of Colomera (IIE) silicate inclusions. *Meteoritics Planet. Sci.* **32**, A61–62.

Hsu W. (2002) Ion probe study of Miles (IIE) silicate inclusions. *Meteoritics Planet. Sci.* **37**, A67.

Ikeda Y. and Prinz M. (1996) Petrology of silicate inclusions in the Miles IIE iron. *Proc. NIPR Symp. Antarct. Meteorites* **9**, 143–173.

Ikeda Y., Ebihara M., and Prinz M. (1997) Petrology and chemistry of the Miles IIE iron. I. Description and petrology of twenty new silicate inclusions. *Antarct. Meteorite Res.* **10**, 355–372.

Lodders K. and Fegley B. (1993) Lanthanide and actinide chemistry at high C/O ratios in the solar nebula. *Earth Planet. Sci. Lett.* **177**, 125–145.

McKay G., Wagstaff J., and Yang S.-R. (1986) Clinopyroxene REE distribution coefficients for shergottites: The REE content of the Shergotty melt. *Geochim. Cosmochim. Acta* **50**, 927–937.

Meibom A. and Clark B. E. (1999) Evidence for the insignificance of ordinary chondritic material in the asteroid belt. *Meteoritics Planet. Sci.* **34**, 7–24.

Niemeyer S. (1980) I-Xe and ^{40}Ar-^{39}Ar dating of silicate from Weekeroo Station and Netschaëvo IIE iron meteorites. *Geochim. Cosmochim. Acta* **44**, 33–44.

Oe K., McKay G., and Le L. (2001) REE and strontium partition coefficients for Nakhla pyroxenes. *Lunar Planet. Sci.* **XXXII,** abstract #2174. Lunar and Planetary Institute, Houston (CD-ROM).

Olsen E., Davis A., Clarke R. S., Schultz L., Weber H. W., Clayton R., Mayeda T., Jarosewich E., Sylvester P., Grossman L., Wang M. Lipschutz M. E., Steele I. M., and Schwade J. (1994) Waston: A new link in the IIE iron chain. *Meteoritics* **29,** 200–213.

Olsen E. and Jarosewich E. (1971) Chondrules: First occurrence in an iron meteorite. *Science* **174**, 583–585.

Palme H., Suess H., and Zeh H. D. (1981) Abundance of the elements in the solar system. In *Astronomy and Astrophysics* (ed. Landolt-Börnstein), pp. 257–272. Springer-Verlag.

Ruzicka A., Fowler G. W., Snyder G. A., Prinz M., Papike J. J., and Taylor L. A. (1999) Petrogenesis of silicate inclusions in the Weekeroo Station IIE iron meteorite: Differentiation, remelting, and dynamic mixing. *Geochim. Cosmochim. Acta* **63**, 2123–2143.

Sanz H. G., Burnett D. S., and Wasserburg G. J. (1970) A precise ^{87}Rb/^{87}Sr age and initial ^{87}Sr/^{86}Sr for the Colomera iron meteorite. *Geochim. Cosmochim. Acta* **34**, 1227–1239.

Schwandt C. S. and McKay G. A. (1996) REE partition coefficients from synthetic diogenite-like enstatite and the implications of petrogenetic modeling. In *Workshop on evolution of igneous asteroids: Focus on Vesta and the HED meteorites.* LPI Tech. Report 96-02, 25–26.

Snyder G. A., Lee D.-C., Ruzicka A. M., Prinz M., Taylor L. A., and Halliday A. N. (2001) Hf-W, Sm-Nd, and Rb-Sr isotopic evidence of late impact fractionation and mixing of silicates on iron meteorite parent bodies. *Earth Planet. Sci. Lett.* **186**, 311–324.

Takeda H., Hsu W., Huss G., and Wasserburg G. J. (1998) Silicate inclusions in the Colomera IIE iron and segregation of partial melts. *Lunar Planet. Sci.* **XXIX,** abstract #1677. Lunar and Planetary Institute, Houston (CD-ROM).

Takeda MH., Hsu W., and Huss G. (in press). Mineralogy of silicate inclusions of the Colomera IIE iron and crystallization of Cr-diopside and alkali feldspar from a partial melt. *Geochim. Cosmochim. Acta* (in press).

Wasserburg G. J., Sanz H. G., and Bence A. E. (1968) Potassium-feldspar phenocrysts in the surface of Colomera, and iron meteorite. *Science* **161**, 684–687.

Wasson J. T. and Wang J. (1986) A nonmagmatic origin of group-IIE iron meteorites. *Geochim. Cosmochim. Acta* **50**, 725–732.

Zinner E. and Crozaz G. (1986) A method for the quantitative measurement of rare earth elements in the ion microprobe. *Int. J. Mass Spectr. Ion Processes* **69**, 17–38.

Appendix 1. Trace element concentrations (ppm) of Miles silicate inclusions.

	Miles 4866-3 i1						
	Diopside	Orthopyroxene	Whitlockite			Apatite	
	Diop1-1	Opx1-1	Whit1-1	Whit1-2	Whit1-3	Apat1-1	Apat1-2
Y	7.214 ± 0.280	0.735 ± 0.030	824.2 ± 3.4	423.4 ± 3.3	220.5 ± 2.2	128.9 ± 1.0	129.0 ± 0.9
La	0.220 ± 0.017	0.006 ± 0.001	397.8 ± 3.2	417.1 ± 4.4	336.6 ± 3.7	67.7 ± 1.0	68.2 ± 0.9
Ce	0.897 ± 0.058	0.012 ± 0.003	1204.2 ± 6.1	1214.9 ± 8.3	909.3 ± 6.8	199.1 ± 1.8	200.3 ± 1.7
Pr	0.159 ± 0.012	0.000 ± 0.000	190.4 ± 2.2	178.8 ± 2.9	133.6 ± 2.4	28.4 ± 0.6	27.4 ± 0.6
Nd	0.982 ± 0.042	0.029 ± 0.004	757.0 ± 5.3	738.2 ± 7.2	476.9 ± 5.5	111.4 ± 1.6	112.7 ± 1.4
Sm	0.470 ± 0.041	0.010 ± 0.004	185.4 ± 2.3	160.9 ± 4.5	105.9 ± 3.6	26.9 ± 1.2	27.5 ± 1.1
Eu	0.068 ± 0.009	0.002 ± 0.001	2.2 ± 0.1	2.2 ± 0.2	2.7 ± 0.2	1.4 ± 0.1	1.2 ± 0.1
Gd	1.084 ± 0.066	0.053 ± 0.014	152.8 ± 4.8	107.2 ± 6.2	47.7 ± 4.5	23.5 ± 1.3	23.3 ± 1.2
Tb	0.193 ± 0.015	0.014 ± 0.003	28.7 ± 0.9	20.0 ± 1.5	10.7 ± 1.1	4.8 ± 0.3	4.8 ± 0.3
Dy	0.965 ± 0.044	0.087 ± 0.008	154.5 ± 1.6	106.6 ± 3.0	56.6 ± 2.1	22.3 ± 0.7	20.6 ± 0.6
Ho	0.267 ± 0.016	0.026 ± 0.004	26.2 ± 0.5	19.4 ± 1.0	8.5 ± 0.6	4.0 ± 0.2	3.3 ± 0.2
Er	0.742 ± 0.031	0.125 ± 0.010	74.4 ± 0.8	46.6 ± 1.7	20.3 ± 0.9	11.8 ± 0.5	10.4 ± 0.4
Tm	0.143 ± 0.013	0.040 ± 0.005	9.7 ± 0.2	6.3 ± 0.2	3.1 ± 0.1	1.3 ± 0.1	1.2 ± 0.1
Yb	0.714 ± 0.032	0.187 ± 0.011	67.2 ± 0.8	55.3 ± 2.0	31.8 ± 1.2	5.8 ± 0.4	8.1 ± 0.5
Lu	0.089 ± 0.012	0.035 ± 0.005	2.2 ± 0.2	4.9 ± 0.5	1.6 ± 0.2	1.0 ± 0.2	1.3 ± 0.2

Errors quoted reflect 1σ standard deviation from counting statistics only.

Appendix 1. Trace element concentrations (ppm) of Miles silicate inclusions.

	Miles 4866-3 i2			Miles 4866-3 i3			
	Orthopyroxene	Feldspar		Albitic glass		Diopside	Feldspar
	Opx2-1	Ab2-1	Ab2-2	Glass3-1	Glass3-2	Diop3-1	Kfeld3-1
Y	4.375 ± 0.175	0.042 ± 0.006	0.098 ± 0.008	0.068 ± 0.006	0.040 ± 0.004	9.882 ± 0.302	0.025 ± 0.004
La	0.023 ± 0.004	0.185 ± 0.011	0.194 ± 0.010	0.297 ± 0.010	0.303 ± 0.012	0.444 ± 0.023	0.007 ± 0.001
Ce	0.084 ± 0.007	0.207 ± 0.014	0.223 ± 0.011	0.378 ± 0.013	0.366 ± 0.013	1.352 ± 0.049	0.012 ± 0.003
Pr	0.015 ± 0.003	0.018 ± 0.003	0.024 ± 0.004	0.025 ± 0.003	0.025 ± 0.003	0.234 ± 0.013	0.001 ± 0.001
Nd	0.156 ± 0.011	0.059 ± 0.008	0.054 ± 0.007	0.105 ± 0.009	0.107 ± 0.008	1.687 ± 0.049	0.010 ± 0.003
Sm	0.139 ± 0.015	0.010 ± 0.007	0.021 ± 0.007	0.011 ± 0.007	0.010 ± 0.005	0.807 ± 0.050	0.011 ± 0.005

	Miles 4866-3 i2			Miles 4866-3 i3			
	Orthopyroxene	Feldspar		Albitic glass		Diopside	Feldspar
	Opx2-1	Ab2-1	Ab2-2	Glass3-1	Glass3-2	Diop3-1	Kfeld3-1
Eu	0.020 ± 0.004	0.375 ± 0.031	0.518 ± 0.029	0.658 ± 0.017	0.555 ± 0.016	0.106 ± 0.010	0.097 ± 0.009
Gd	0.279 ± 0.032	0.021 ± 0.009	0.006 ± 0.006	0.019 ± 0.006	0.009 ± 0.006	1.668 ± 0.087	0.005 ± 0.003
Tb	0.071 ± 0.008					0.312 ± 0.017	
Dy	0.510 ± 0.021					1.743 ± 0.044	
Ho	0.144 ± 0.009					0.365 ± 0.018	
Er	0.671 ± 0.025					1.176 ± 0.037	
Tm	0.133 ± 0.009					0.176 ± 0.015	
Yb	0.823 ± 0.026					1.115 ± 0.036	
Lu	0.152 ± 0.016					0.143 ± 0.013	

Appendix 1. Trace element concentrations (ppm) of Miles silicate inclusions.

	Miles 4866-4 i4						
	Albitic glass			Diopside			
	Glass4-1	Glass4-2	Glass4-3	Diop4-1	Diop4-2	Diop4-3	Diop4-4
Y	0.663 ± 0.035	0.666 ± 0.035	0.707 ± 0.033	6.403 ± 0.230	8.218 ± 0.287	9.573 ± 0.290	13.169 ± 0.295
La	0.032 ± 0.004	0.046 ± 0.004	0.027 ± 0.003	0.107 ± 0.009	0.133 ± 0.011	0.204 ± 0.013	0.367 ± 0.020
Ce	0.052 ± 0.006	0.062 ± 0.006	0.049 ± 0.004	0.381 ± 0.021	0.619 ± 0.024	0.972 ± 0.030	1.891 ± 0.113
Pr	0.006 ± 0.002	0.006 ± 0.002	0.005 ± 0.001	0.135 ± 0.010	0.147 ± 0.011	0.201 ± 0.012	0.279 ± 0.015
Nd	0.038 ± 0.006	0.040 ± 0.006	0.036 ± 0.005	0.791 ± 0.032	0.988 ± 0.038	1.294 ± 0.042	2.267 ± 0.069
Sm	0.014 ± 0.005	0.020 ± 0.007	0.007 ± 0.004	0.513 ± 0.038	0.536 ± 0.041	0.763 ± 0.046	1.322 ± 0.055
Eu	0.072 ± 0.012	0.092 ± 0.013	0.012 ± 0.009	0.067 ± 0.008	0.064 ± 0.009	0.099 ± 0.008	0.179 ± 0.010
Gd	0.029 ± 0.008	0.052 ± 0.009	0.035 ± 0.007	0.872 ± 0.082	1.058 ± 0.069	1.721 ± 0.075	2.561 ± 0.104
Tb	0.006 ± 0.002	0.009 ± 0.002	0.009 ± 0.001	0.166 ± 0.013	0.195 ± 0.015	0.311 ± 0.018	0.430 ± 0.018
Dy	0.061 ± 0.006	0.062 ± 0.007	0.057 ± 0.006	1.062 ± 0.036	1.074 ± 0.037	1.747 ± 0.043	2.260 ± 0.077
Ho	0.020 ± 0.004	0.019 ± 0.005	0.016 ± 0.003	0.234 ± 0.014	0.274 ± 0.016	0.395 ± 0.017	0.386 ± 0.018
Er	0.054 ± 0.008	0.081 ± 0.008	0.056 ± 0.005	0.724 ± 0.030	0.669 ± 0.030	1.141 ± 0.036	1.414 ± 0.040
Tm	0.010 ± 0.002	0.008 ± 0.003	0.010 ± 0.002	0.110 ± 0.011	0.108 ± 0.011	0.154 ± 0.012	0.209 ± 0.013
Yb	0.025 ± 0.004	0.055 ± 0.007	0.018 ± 0.003	0.630 ± 0.027	0.709 ± 0.032	1.007 ± 0.034	0.895 ± 0.033
Lu	0.017 ± 0.003	0.021 ± 0.003	0.021 ± 0.004	0.059 ± 0.009	0.076 ± 0.011	0.143 ± 0.013	0.132 ± 0.011

Appendix 1. (continued)

Miles 4866-4 i4					
Orthopyroxene			Whitlockite		
Opx4-1	Opx4-2	Opx4-3	Whit4-1	Whit4-2	Whit4-3
1.243 ± 0.078	1.161 ± 0.014	0.424 ± 0.009	85.7 ± 0.8	95.7 ± 0.9	81.0 ± 0.8
0.010 ± 0.002	0.004 ± 0.001	0.001 ± 0.001	19.0 ± 0.5	19.0 ± 0.5	17.0 ± 0.5
0.062 ± 0.005	0.018 ± 0.002	0.006 ± 0.002	46.1 ± 0.9	45.0 ± 0.9	43.9 ± 0.9
0.010 ± 0.002	0.004 ± 0.001	0.001 ± 0.001	6.6 ± 0.3	6.5 ± 0.3	6.7 ± 0.3
0.080 ± 0.007	0.043 ± 0.004	0.003 ± 0.002	29.7 ± 0.7	31.1 ± 0.7	29.7 ± 0.7
0.035 ± 0.008	0.012 ± 0.003	0.005 ± 0.003	10.4 ± 0.4	10.4 ± 0.5	10.0 ± 0.4
0.015 ± 0.003	0.003 ± 0.003	0.003 ± 0.001	3.4 ± 0.1	3.5 ± 0.1	3.4 ± 0.1
0.115 ± 0.014	0.085 ± 0.013	0.007 ± 0.002	13.4 ± 0.8	12.7 ± 0.9	11.2 ± 0.8
0.025 ± 0.003	0.024 ± 0.003	0.003 ± 0.001	2.3 ± 0.2	2.2 ± 0.2	2.2 ± 0.2
0.170 ± 0.010	0.161 ± 0.008	0.047 ± 0.005	15.0 ± 0.5	14.4 ± 0.6	12.5 ± 0.5
0.042 ± 0.004	0.047 ± 0.003	0.014 ± 0.002	2.7 ± 0.1	2.9 ± 0.1	2.4 ± 0.1
0.149 ± 0.010	0.186 ± 0.008	0.070 ± 0.006	7.4 ± 0.2	8.1 ± 0.3	6.4 ± 0.2
0.032 ± 0.004	0.038 ± 0.004	0.014 ± 0.003	1.1 ± 0.0	1.1 ± 0.1	1.0 ± 0.0
0.225 ± 0.012	0.032 ± 0.005	0.037 ± 0.004	8.1 ± 0.2	7.6 ± 0.2	7.0 ± 0.2
0.044 ± 0.006	0.040 ± 0.004	0.034 ± 0.004	1.0 ± 0.1	1.0 ± 0.1	0.9 ± 0.1

Appendix 1. Trace element concentrations (ppm) of Miles silicate inclusions.

	Miles 4866-4 i5				Miles 4866-4 i6			Miles 4866-5 i7	
	Diopside	Orthopyroxene	Feldspar		Apatite	Albitic glass	Orthopyroxene	Albitic glass	
	Diop5-1	Opx5-1	Ab5-1	Ab5-2	Apat5-1	Glass6-2	Opx6-1	Glass 7-1	Glass 7-2
Y	24.256 ± 0.377	3.484 ± 0.127	0.379 ± 0.015	1.031 ± 0.047	182.9 ± 1.3	0.564 ± 0.023	5.467 ± 0.152	0.296 ± 0.013	0.327 ± 0.014
La	0.967 ± 0.050	0.005 ± 0.001	0.531 ± 0.017	0.619 ± 0.027	71.4 ± 1.1	0.031 ± 0.004	0.006 ± 0.001	0.856 ± 0.032	0.714 ± 0.029
Ce	4.472 ± 0.230	0.024 ± 0.003	0.701 ± 0.020	1.348 ± 0.051	189.5 ± 1.9	0.087 ± 0.007	0.024 ± 0.003	1.077 ± 0.036	0.971 ± 0.036
Pr	0.945 ± 0.044	0.005 ± 0.002	0.062 ± 0.005	0.125 ± 0.009	26.8 ± 0.7	0.011 ± 0.003	0.005 ± 0.001	0.075 ± 0.005	0.088 ± 0.007
Nd	5.224 ± 0.136	0.048 ± 0.006	0.227 ± 0.014	0.519 ± 0.026	121.1 ± 1.7	0.058 ± 0.007	0.071 ± 0.007	0.278 ± 0.016	0.330 ± 0.017
Sm	2.323 ± 0.077	0.042 ± 0.007	0.084 ± 0.015	0.068 ± 0.018	28.8 ± 1.3	0.022 ± 0.006	0.028 ± 0.008	0.038 ± 0.010	0.050 ± 0.012
Eu	0.102 ± 0.011	0.003 ± 0.002	0.449 ± 0.045	0.601 ± 0.057	1.4 ± 0.1	0.104 ± 0.008	0.000 ± 0.002	0.417 ± 0.025	0.404 ± 0.024
Gd	4.255 ± 0.218	0.129 ± 0.017	0.027 ± 0.010	0.097 ± 0.018	32.8 ± 1.6	0.032 ± 0.009	0.222 ± 0.025	0.025 ± 0.010	0.016 ± 0.010
Tb	0.684 ± 0.037	0.040 ± 0.004			5.6 ± 0.4	0.011 ± 0.003	0.070 ± 0.006		
Dy	4.075 ± 0.111	0.346 ± 0.014			29.0 ± 0.9	0.083 ± 0.008	0.429 ± 0.017		
Ho	0.872 ± 0.043	0.108 ± 0.007			5.9 ± 0.3	0.022 ± 0.003	0.178 ± 0.009		
Er	2.556 ± 0.084	0.496 ± 0.017			14.3 ± 0.5	0.063 ± 0.008	0.581 ± 0.021		
Tm	0.354 ± 0.016	0.111 ± 0.007			1.5 ± 0.1	0.012 ± 0.004	0.094 ± 0.008		
Yb	2.316 ± 0.057	0.747 ± 0.020			8.9 ± 0.3	0.011 ± 0.003	0.808 ± 0.024		
Lu	0.314 ± 0.017	0.125 ± 0.008			1.4 ± 0.1	0.017 ± 0.004	0.173 ± 0.010		